AnT^{2}COK, an analytical model for cyclic oxidation kinetics of hot-work tool steels in transient thermal cycling conditions

Gilles Dour, Mehdi Salem, Sabine Le Roux, Damien Texier, Farid Medjedoub, Pascal Lamesle, Farhad Rezai-Aria

AnT^{2}COK, an analytical model for cyclic oxidation kinetics of hot-work tool steels in transient thermal cycling conditions

G. Dour*[,1], M. Salem, S. Le Roux, D. Texier*, F. Medjedoub[2], P. Lamesle[3], F. Rézaï-Aria

Institut Clément Ader (ICA), Université de Toulouse, CNRS, INSA, UPS, Mines Albi, ISAE-SUPAERO, Campus Jarlard, 81013 Albi Cedex 09, France

A B S T R A C T

In hot forming processes, steel tools are subjected to rapid temperature transients and cyclic oxidation. AnT^{2}COK, a new analytical model based on diffusion-controlled oxide growth in cyclic conditions, is proposed to predict the parabolic oxidation kinetics in spallation-free conditions. Compared to cyclic oxidation models of the literature (COREST, COSP, DICOSM, etc.), it is applicable for any shape of thermal cycle, fully transient or with dwell time. The model is applied to thermal fatigue tests on X38CrMoV5 steel, for T_{max} between 500 and 685 °C. Its validity is demonstrated above 550 °C, using frequency factor and activation energy calculated from isothermal tests.

Keywords:
Tool steel
Modeling
SEM
Thermal cycling
High temperature corrosion
Cyclic oxidation

1. Introduction

Chromium martensitic steels (e.g. AISI H11 and H13 grades) are commonly used as tool materials (molds, dies or rolls) in high-temperature forming processes, as for example hot forging, drop forging, stamping, hot-extrusion, die casting, hot-rolling, etc. [1–7]. During these manufacturing operations, the tools are not only subjected to elevated temperatures, but also experience large transient thermal fluctuations when the surface comes into contact with the shaped part (or the molten alloy) at each production cycle or during start-up and shut-down operations. These cyclic temperature variations are often extremely fast, thus inducing severe thermal gradients within the tool, which give rise to stresses and strains in a shallow region beneath the contact surface [8,9]. For example, in high-pressure die casting, a large quantity of heat is exchanged in a very short time during the intimate contact between the molten alloy and the die surface [9–11]. This input energy provokes a transient thermal situation, and the thermal expansions and contractions through the die wall are not uniform. The repetition of production cycles leads to the tooling damage by thermal fatigue, which was defined by Spera [12] as *"the gradual deterioration and eventual cracking of the material by alternate heating and cooling during which free thermal expansion is partially or completely constrained"*. In fact, the die wall is subjected to a thermo-mechanical stress-strain hysteresis loop where the external surface goes into compression during the heating phase, and into tension during the cooling phase. Most hot-work tool applications therefore require using tool materials with a good resistance to thermal fatigue at high temperature, i.e. to oxidation and crack initiation/propagation [13–16].

In addition, the cyclic thermo-mechanical solicitations are often coupled with severe atmospheres which subject the tools to oxidation or corrosion reactions [16–19]. It is widely accepted that oxidation plays a major role in the initiation stage of thermal fatigue cracking [13–16,20–22]. In thermal fatigue conditions, the growth of the multi-oxide layer is generally followed by the formation of a superficial network of micro-cracks (often named "heat-checking") on the tool or specimen surface, due to the repetitive thermal stresses [14,15,20–22]. By increasing the number of cycles, these through-oxide cracks can initiate some macro-cracks propagating into the steel [13–16,20–24]. Given the importance of oxidation in thermal fatigue, extensive research has been devoted to studying the oxidation behavior of metallic alloys under isothermal and cyclic conditions [16,19,25–39].

In the literature, the term "cyclic oxidation" usually refers to tests in which the samples are subjected to repeated cycles of heating (to a maximum temperature) and cooling (to a minimum temperature), with a significant dwell time at the maximum temperature. These tests often result in a spallation mechanism in which a local rupture of the oxide layer and possibly a net loss of mass take place, due to local stresses at the oxide/metal interface [27,28,34,35,38,40]. Under these conditions,

* Corresponding authors.
E-mail addresses: gretchgilles@netspace.net.au (G. Dour), damien.texier@mines-albi.fr (D. Texier).
[1] Present address: Advisian, Worley Parsons, 600 Murray Street, West Perth, WA 6005, Australia.
[2] Present address: Airbus France, Site de Saint Martin du Touch, 316 Route de Bayonne, 31060 Toulouse Cedex 9, France.
[3] Present address: IRT-M2P, Bâtiment CIRAM, 4 rue Augustin Fresnel, 57070 Metz, France.

Nomenclature

A	equivalent oxidation time
Hr	heating rate of the thermal cycle
ht	heating period of the thermal cycle
k	series/cycles iteration integer
k_p k_p'	apparent oxidation rate constant (or parabolic constant)
k_0 k_0'	pre-exponential factor (or frequency factor)
k_0^{isoth} k_0^{cycl}	pre-exponential factor in isothermal or cyclic conditions
N	total number of thermal cycles
Q Q'	activation energy
Q_h	activation energy for temperatures higher than 550 °C
Q_l	activation energy for temperatures lower than 550 °C
R	universal gas constant
Ra	arithmetic average roughness
t, t'	time
t_{cy}	cycle time
t_{ei}	equivalent time at T (time necessary to grow an oxide layer δ_{ox} at T)
T	temperature
T_{min} T_{max}	minimum and maximum temperature of the thermal cycle
δ_{ox}	thickness of the oxide layer
Φ_{max}	maximum heat-flux density

the modeling is based on the quantification of both mass gains by oxidation and mass loss by spallation in cyclic conditions [43–47].

However, spallation does not always occur in thermal cycling. Robertson and Manning [41] have indeed proposed a series of failure mode maps depending on strain and oxide thickness for various oxide systems. They defined several regions, i.e. scale integrity, spalling and delamination, and through-scale cracking. Nagl and Evans [42] also identified failure mechanisms for oxides under tensile stress and revealed that the oxides break up into a finite number of segments at the region of high stress concentration. Neu and Sheitoglu [25] found that spallation-free oxide could be observed at low strain rates. They showed a relationship between both temperature and applied fatigue strain rate, and the type of oxides. In the particular case examined in the present study (i.e. thermal fatigue of hot-work tool steels), the oxide layer formed on the specimen spalled only in a restricted number of conditions: (i) in regions with a high curvature (geometrical singularities of the cylindrical specimen), and (ii) for thermal cycles with a low maximum temperature (< 550 °C) [9,16,22]. All experimental data were collected in the central area of the specimen where spallation-free conditions are met. Indeed, they all fell in the low strain rate range (for the studied temperature range) and in low curvature regions.

The purpose of this paper is to describe and validate a new analytical model allowing the quantification of oxide thickness growth, in non-isothermal conditions without spallation and for a severe transient thermal cycling (with alternate heating/cooling phases). The model is developed to account for the cyclic growth of any diffusion-controlled oxide governed by parabolic kinetics, during thermal cycle that can be of any shape (i.e. incorporating a dwell or not). It is here applied to thermal fatigue tests performed under various conditions without any dwell, on a X38CrMoV5 hot work tool steel grade, also known as *AISI H11*. Its validity is analyzed based on oxidation data produced in our laboratory.

The proposed analytical model, denoted AnT^{2}COK for Analytical Thermal Transient Cyclic Oxidation Kinetics, has significant differences with more classical cyclic oxidation conditions and models, where:

- the tests are usually performed with a temperature ramp-up, a long dwell at the maximum temperature and then a fast cooling stage before restarting the cycle [34,35,43–47], whereas our tests are fully transient;
- a low number of cycles (usually less than hundred cycles) is applied [35,43–47], compared to several ten thousand cycles in our thermal fatigue tests;
- most models, such as COREST (by Barrett and Presler [43]), COSP (by Lowell et al. [44]), DICOSM (by Smialek [45]) or P-kp (by Poquillon and Monceau [46]), are founded on the mass gain obtained in isothermal condition at the dwell temperature. They also take into account the slowing effect of the oxide layer already formed during the previous cycles. However, such models are well relevant to the experimental conditions examined by these authors and the targeted applications (turbine components), but not to the conditions encountered in hot-work tool applications where the thermal transient phase cannot be ignored;
- Raffaitin et al. [34] included the oxidation mass gain in the fast transient heating and cooling phases, but considered the net mass gain as an input data measured during thermo-gravimetric experiments rather than modeling.

2. Theory

In spallation-free cyclic oxidation, the difficulty for modeling the oxide growth is to account for the shape of thermal cycles. Should the oxide growth be controlled by diffusion, it may be possible to fit a parabolic law for conditions that are very similar. In the COSP-type models, a parabolic behavior can usually be observed before spallation takes place. However, as demonstrated by Raffaitin et al. [34] with a continuous recording of the mass gain during thermal cycles, the oxidation growth within the transient phases can be complex. For thermal cycles in which the transient periods are dominating, modeling the oxide growth is challenging.

The present model, AnT^{2}COK, is intended to account for the shape of any thermal cycle, provided that the following assumptions are met:

1 no spallation takes place;
2 the oxidation kinetics of the metallic material (here a tool steel) is controlled by diffusion, and the growth of the oxide layer follows a parabolic law in isothermal conditions;
3 in the Arrhenius law, the frequency factor - which is linked to the density of diffusion path - is independent of the shape and temperature range of the thermal cycles.

Given these assumptions, it is accepted that the diffusion-controlled oxide growth follows a parabolic law, as expressed by:

$$\delta_{ox}(t) = k_p . \sqrt{t} \tag{1}$$

where δ_{ox} is the oxide thickness, k_p is the apparent oxidation rate constant (parabolic constant), and t is the oxidation time.

The apparent oxidation rate constant k_p, which is temperature-dependent, is given by the Arrhenius law:

$$k_p = k_0 . exp\left(-\frac{Q}{RT}\right) \tag{2}$$

where k_0 is a pre-exponential factor also called frequency factor (expressed in $\mu m.s^{-1/2}$), Q is the activation energy (in $J.mol^{-1}$), R is the universal gas constant ($8.314\ J.mol^{-1}.K^{-1}$) and T is the absolute temperature (in K).

In cyclic conditions, the time t represents the total duration of the cyclic test and can be calculated as the product of the cycle time t_{cy} by the total number of cycles N:

$$t = t_{cy} . N \tag{3}$$

Assuming that the parabolic rate and the Boltzmann law for the

coefficient both apply at any time (as in the CORREST, COSP and DICOSM models [43–45]), Eqs. (1) and (2) should apply for any one isothermal step lasting a time t' after a number of cycles leading to a pre-existing oxide layer. This can be expressed by the following equations, for two consecutive time steps t and $(t + t')$:

$$\delta_{ox}(t + t') = k_0 . exp\left(-\frac{Q}{RT}\right) . \sqrt{t' + t_{ei}} \tag{4}$$

where t is the actual time at the start of the isothermal step, t' is the time in the isothermal step (starting at 0 when the step starts), and t_{ei} is the time it would take to grow an oxide layer of the initial thickness $\delta_{ox}(t_{ei})$ at the temperature T, in isothermal conditions.

Extrapolating this for an infinitesimal isothermal step of duration ∂t, which may be preceded by other isothermal steps at different temperatures, one can express the growth rate during the step ∂t by differencing Eq. 4 to the time (all other parameters being kept at a constant value), and t' being set to 0 (beginning of the new isothermal step):

$$\left[\frac{\partial \delta_{ox}}{\partial t}\right]_{T,t} = \frac{\partial}{\partial t}\left[k_0 . exp\left(-\frac{Q}{RT}\right) . \sqrt{t' + t_{ei}}\right]_{T,t} \tag{5}$$

where the bracket followed by "T, t" means isothermal step at the time t and at temperature T (for a transformation at constant temperature).

In the cyclic oxidation models of the literature [35,44], the derivation term is replaced by the derivation of the square root of time for $t' = 0$, considering that T is constant during the time step ∂t.

$$\left[\frac{\partial \delta_{ox}}{\partial t}\right]_{T,t} = \left[\frac{k_0}{2\sqrt{t_{ei}}} . exp\left(-\frac{Q}{RT}\right)\right]_{T,t} \tag{6}$$

As aforementioned, the term t_{ei} is the time it would take to grow the oxide formed at the time t for an isothermal dwell at the temperature T to the size that has actually been reached at time t. Numerically, this term is hence related to the oxide thickness at t and the isothermal oxide growth given by Eq. 1, therefore:

$$t_{ei} = \left[\frac{\delta_{ox}(t)}{k_0 . exp\left(-\frac{Q}{RT}\right)}\right]^2 \tag{7}$$

Replacing t_{ei} in Eq. 6 and separating the terms in δ_{ox} from the terms in t, it comes:

$$\delta_{ox}(t) . d\delta_{ox} = \frac{{k_0}^2}{2} . exp\left(-\frac{Q}{RT(t)}\right) dt \tag{8}$$

Eq. 8 can be integrated side by side, giving:

$$\frac{1}{2}(\delta_{ox}(t)^2 - \delta_{ox}(0)^2) = \int_0^t \frac{{k_0}^2}{2} . exp\left(-\frac{2Q}{RT(t)}\right) dt \tag{9}$$

In cyclic conditions where the temperature cycle repeats itself every t_{cy}, Eq. 9 applied at the end of N cycles (t being given by Eq. 3), and the integral in the second term is no more than N times the integral from 0 to t_{cy}. For a non-oxidized specimen at the start of the thermal cycles, it comes:

$$\frac{1}{2}\delta_{ox}(N . t_{cy})^2 = N . \int_0^{t_{cy}} \frac{{k_0}^2}{2} . exp\left(-\frac{2Q}{RT(t)}\right) dt \tag{10}$$

The cyclic oxide growth kinetics for N cycles can then be written in a simple way as:

$$\delta_{ox}(t) = k_0 . \sqrt{\frac{A}{t_{cy}}} . \sqrt{t} \tag{11}$$

or similarly

$$\delta_{ox}(t) = k_0 . \sqrt{A} . \sqrt{N} \tag{12}$$

with the term A equal to:

$$A = \int_0^{t_{cy}} exp\left(-\frac{2Q}{RT(t)}\right) dt \tag{13}$$

It can be noted that Eq. 13 is close to the one proposed by Neu and Sheitoglu [25] for spallation-free oxide growth, but for the power 2 in the exponential. Interestingly, the model of cyclic oxide growth proposed here and called AnT^{2}COK, remains a parabolic law with a moderation factor $\sqrt{A/t_{cy}}$. As expressed in Eq. 13, A represents a time which takes into account the shape of the thermal cycle through the integral, in particular the expression $T(t)$. Since no assumptions were made on the shape of the thermal cycle, it can be applied to any types of cycles (fully transient or transient with dwell time). Thereafter, this time will be called the "equivalent oxidation time" of the thermal cycle. Its expression recalls the notion of time-temperature equivalence, but here applied to a thermal cycle.

The time necessary to form an oxide of thickness δ_{ox} will be investigated taking into account either:

- (i) the full time of the cycle t,
- (ii) an effective oxidation time (t') corresponding only to the time of the cycle above 300 °C, which can be considered as an inferior limit of "high temperature". Indeed, several experimental works in our laboratory showed a negligible contribution of the oxidation below 300 °C in this temperature range for a X38CrMoV5 tool steel grade,
- (iii) the "equivalent oxidation time" of the thermal cycle A defined in the AnT^{2}COK model, with one set of activation energy Q and frequency factor k_0,
- (iv) the "equivalent oxidation time" of the thermal cycle A defined in the AnT^{2}COK model, with two sets of activation energy (Q_l, Q_h) and frequency factor ($k_{0,l}$,$k_{0,h}$). Indeed, two oxidation regimes were found below and above 550–600 °C [48].

3. Experimental methods

3.1. Material

The experiments were performed on a X38CrMoV5 tool steel grade. Its chemical composition, analyzed by Optical Emission Spectrometry (OES) and given in Table 1, is characterized by low carbon (about 0.4%) and high chromium (5%) contents. This alloy is a highly alloyed steel, with strong carbide forming elements (such as molybdenum, vanadium) and a silicon content lower than 1%.

All test specimens were machined from steel bars purchased from Aubert & Duval in annealed condition, cut and heat-treated by Balzers-France. The steel was austenitized under vacuum at 990 °C during 90 min and air quenched. Then, a double-tempering treatment was performed during 90 min at 544 °C and 65 min at either 595 or 600 °C. This complex heat-treatment gave a tempered martensitic microstructure and a final hardness of either 42 or 47 HRC, depending on the second tempering temperature.

3.2. Thermal aging tests (isothermal conditions)

Oxidation kinetics of metallic materials, such as 5% chromium tool steels, is commonly determined in isothermal conditions [30,31]. In this study, thermal aging experiments were performed under isothermal conditions (at nil applied stress) [23,49]. Disc-shaped specimens with a diameter of 40 mm and a thickness of 10 mm, polished to achieve a mean arithmetic roughness (R_a) of 0.03 µm, were used. The specimens

Table 1
Chemical composition of the X38CrMoV5 (AISI H11) steel (in wt.%).

Element	C	Cr	Mo	V	Si	Mn	S	P	Fe
Weight (%)	0.396	5.05	1.25	0.47	0.94	0.36	< 0.003	0.009	*bal.*

were thermally aged in a heat resisting furnace, at five temperature levels (500, 550, 600, 650 and 700 °C) and for various durations (1, 9, 25 and 100 h). The temperature was verified with a K-type thermocouple located on the furnace bed.

3.3. Thermal fatigue tests (thermal transient cyclic conditions)

Thermal fatigue tests were performed using an induction heating system and a 25 kW high frequency generator. Cylindrical-shaped specimens were used, with internal and outer diameters of respectively 10 and 30 mm and a wall thickness of 10 mm. The external surface was mechanically polished to R_a = 0.02 µm. During the test, the specimen was rapidly heated by induction and cooled down by water internal cooling and natural convection in atmospheric air. The temperature was measured by a K-type thermocouple with a wire diameter of 0.1 mm, spot-welded to the external surface in the central part of the specimen. Further measurements were performed using a fully instrumented specimen for validation of the power input against a numerical simulation [9]. The geometry of the specimen, the thermal fatigue rig and the experimental procedure have been described in detail in [9,22].

In this study, various thermal conditions were investigated with a minimum temperature (T_{min}) fixed to 100 °C, and a maximum temperature (T_{max}) varying from 500 to 685 °C. The experimental parameters used for the various thermal conditions are reported in Table 2, and their related temperature-time cycles are depicted in Fig. 1a and b. For the tests performed at T_{max} = 650 °C, various maximum heat-flux densities Φ_{max}, ranging from 2 to 5 MW.m^{-2}, were applied on the surface of the specimen. This leads in different heating periods (*ht*) fine-tuned from 1.5 to 6.3 s to reach 650 °C (Fig. 1b). During the thermal fatigue tests, the temperature gradients generate a thermo-mechanical loading in the specimen, leading to the formation of a crack network (also called "heat-checking") on the oxidized surface. The tests, carried out up to 3,000 to 100,000 cycles depending on the applied thermal cycle, were regularly interrupted in order to observe the evolution of the morphology of the superficial oxide layer formed on the specimen.

3.4. Characterization of the oxide layer

The morphology of the superficial oxide layer formed on both thermal aging and thermal fatigue specimens was observed with a scanning electron microscope (SEM), using a secondary electron (SE) detector. At the end of either the thermal aging or thermal fatigue test, the specimen was electro-coated with a nickel layer, cut, and mirror polished for cross-section observations. SEM observations in a back-scattered electron (BSE) mode, combined with energy dispersive spectroscopy (EDS) analysis, were used to determine the distribution of elements in the oxide layers. Measurements of the mean thickness of the oxide layer were performed by image analysis on twenty micrographs acquired at different positions along the cutting plane, in the central region of the specimen where the temperature is particularly homogeneous [9,22].

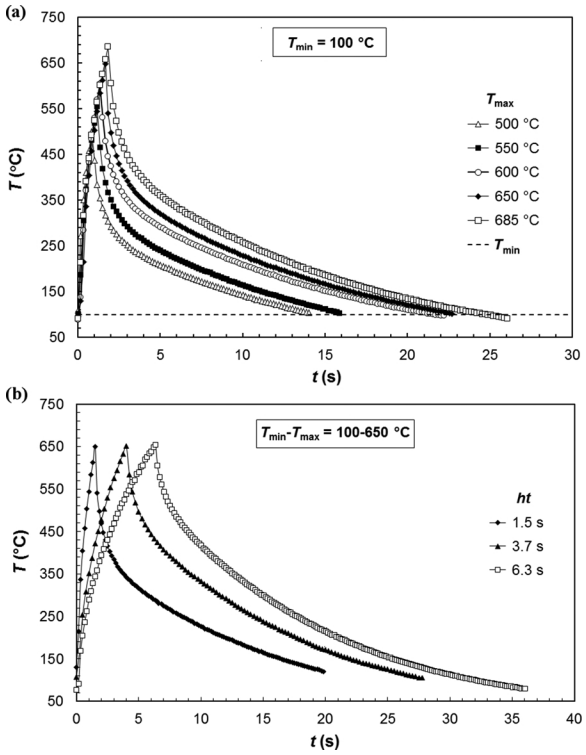

Fig. 1. Temperature-time cycles applied in thermal fatigue experiments: (a) with various maximum temperatures T_{max}, (b) with various heating times *ht*.

In addition, the crystallographic nature of the oxides was identified by X-ray diffraction (XRD) analysis using a Panalytical X'Pert Pro diffractometer with CuK_α radiation (λ = 1.54 Å) and point detector. The parameters used during XRD analyses were an angular step size of 0.033°, an integration time of 15 s, a voltage of 40 kV and a current of 40 mA, in conventional *2θ* acquisition mode. Such parameters were imposed by the complex geometry of the thermal fatigue specimens (edge of a thin wall).

4. Results

4.1. Composition and morphology of the oxide layers

After isothermal aging or thermal fatigue, the microstructure of the oxidized region exhibited a multi-layered structure, with chemical and morphological changes from the surface to the oxide/substrate interface (Fig. 2a). This led to the formation of the following oxide phases, from the outer surface to the steel:

- a superficial layer of hematite (Fe_2O_3), rich in iron and poor in chromium;
- a magnetite (Fe_3O_4) layer;

Table 2
Parameters of the thermal cycles used in the thermal fatigue tests.

Initial roughness of the specimen *Ra* (µm)	Initial hardness of the specimen (HRC)	Thermal cycle T_{min} - T_{max} (°C)	Heating time *ht* (s)	Cooling time *ct* (s)	Cycling duration t_{cy} (s)	Total number of cycles *N* (cycles)
0.02	47	100 - 500	0.7	13.0	13.7	100,000
0.02	47	100 - 550	0.9	14.5	15.4	80,000
0.02	47	100 - 600	1.3	15.0	16.3	80,000
0.02	42 / 47	100 - 650	1.5	17.0	18.5	20,000
0.02	47	100 - 650	3.7	22.0	25.7	30,000
0.02	47	100 - 650	6.3	30.0	36.3	50,000
0.02	42 / 47	100 - 685	1.8	22.0	23.8	3,000

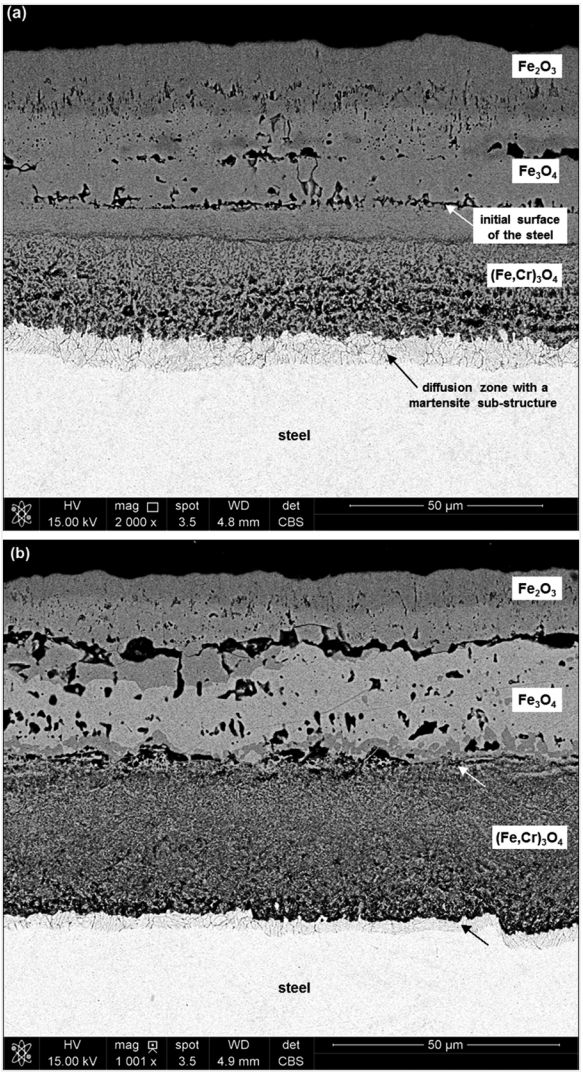

Fig. 2. (a) SEM cross-section observation with a circular backscatter detector, after a chemical etching revealing the microstructure and the morphology of the multi-layered oxide formed on thermally aged samples: a) at 650 °C during 100 h; (b) at 700 °C during 25 h.

- a magnetite-rich spinel oxide ($(Fe,Cr)_3O_4$), enriched in chromium;
- a fine interface just above the steel, depleted in iron and chromium.

These multi-layer structure and composition, found up to 650 °C, are consistent with observations reported in the literature for similar steel grades [29,31,33,36,37]. As confirmed by Fig. 2b, the same composition was found at higher temperatures (700 °C). The limit between the anionic and cationic diffusion grown oxides, clearly visible on the micrographs, corresponds to the initial surface of the steel (as depicted in Fig. 2a and b with a white arrow). In addition, the typical initial microstructure of the steel (laths) may be recognized as a substructure in the diffusion zone (light grey zone next to the steel substrate, highlighted with a black arrow in Fig. 2a and b) [50].

From the EDS profiles (Fig. 3), it was observed:

- a lower oxygen concentration in the outer hematite layer than in the inner layers, where it remains steady until the fine interface just above the steel substrate;
- an absence of chromium in the outer oxide layers (hematite and magnetite).

As shown in Fig. 4, XRD analyses performed on both thermal aging and thermal fatigue specimens confirmed the presence of Fe_2O_3 and Fe_3O_4 on the surface. The spinel oxide, however, could not be differentiated from magnetite because of the overlapping position of their diffraction peaks.

For the thermal fatigue specimens, a multi-directional network of micro-cracks initiated on the surface of the compact and homogeneous oxide layer after a few thousand cycles (Fig. 5a), due to the thermal stresses induced by the thermal cycling [9]. Indeed, the specimen was self-constrained during the test, because the free expansion of the surface was hindered by the bulk material which is at a lower temperature. In addition, the oxide compounds have different thermal expansion coefficients than the steel [22,51], leading to a thermal mismatch between the bulk material and the outer layer. This consequently induces a local mechanical incompatibility responsible for the cracking of the oxide layer. A localized spallation of the oxide layer was occasionally encountered, mainly when T_{max} was below 550 °C. However, it should be emphasized that the spallation-growth cycle was not the common mode of oxide growth and wall thickness consumption in such experiments.

Post-mortem cross-section observations of the same specimen at higher magnification showed that the micro-cracks crossed the whole oxide layer up to the interface with the substrate (Fig. 5b), and sometimes propagated deeper into the steel due to the oxide diffusion. In addition, similar multi-layered oxide structure and composition were found for thermal fatigue specimens, as the one previously reported for thermal aging tests.

The morphology of the superficial oxide layer changed depending on the maximal temperature of the test, either in isothermal (Fig. 6a) or in cyclic (Fig. 6b) conditions. It must be emphasized that only the hematite layer can be observed in these micrographs, which were all made with similar magnifications. In isothermal conditions, fine white needles were growing in different directions inside a more or less densified matrix (Fig. 6a). Observations of the thermally aged specimens, which are not presented here, revealed also that the needles tended to be more numerous for increased oxidation times. In cyclic conditions (thermal fatigue tests), the hematite layer appeared as tangled glitters for low T_{max} ($\leq$ 600 °C), whereas it was alveolar and porous when T_{max} is 650 °C or above (Fig. 6b). The heating rate of the thermal cycle had less effect on the oxide morphology than the T_{max}. However, a higher heating rate tended to increase slightly the density and the length of needles, while the apparent porosity of the matrix remained similar [9]. For a same T_{max} and an equivalent oxidation time, the hematite layer formed under thermal fatigue appeared very different from that formed under thermal aging, indicating that the oxide growth mechanisms may have been influenced by the mechanical loading (here originated by thermal stresses) [9,22–24].

4.2. Oxide growth kinetics

4.2.1. Isothermal conditions

Fig. 7a and b show the evolution of the oxide thickness (δ_{ox}) versus the square root of the oxidation time (t) in isothermal aging tests, for various temperatures ranging from 500 to 700 °C. The kinetics follows a classic parabolic rate law, in agreement with Eq. 1. As indicated in Table 3, the apparent oxidation rate constant k_p, calculated from regression lines in the (δ_{ox} vs. $t^{1/2}$) curves (Fig. 7a), varies from 4.2×10^{-3} µm.s$^{-1/2}$ (for 500 °C) to 2.4×10^{-1} µm.s$^{-1/2}$ (for 700 °C). From such k_p values, it is possible to estimate the activation energy Q using the Arrhenius law (Eq. 2).

The graphical representation of Arrhenius law (Fig. 8) shows that a linear regression of $\ln(k_p)$ over the whole temperature range provides a reasonable fit (coefficient of determination = 0.87) and gives an activation coefficient of 131 kJ mol^{-1}. This value is consistent with those reported by several authors (e.g. 140 kJ mol^{-1} for similar tool steels [23,49], 125 kJ mol^{-1} for pure iron [52], and 156 kJ mol^{-1} for AISI 1070 steel [26] under isothermal static experiments at nil external

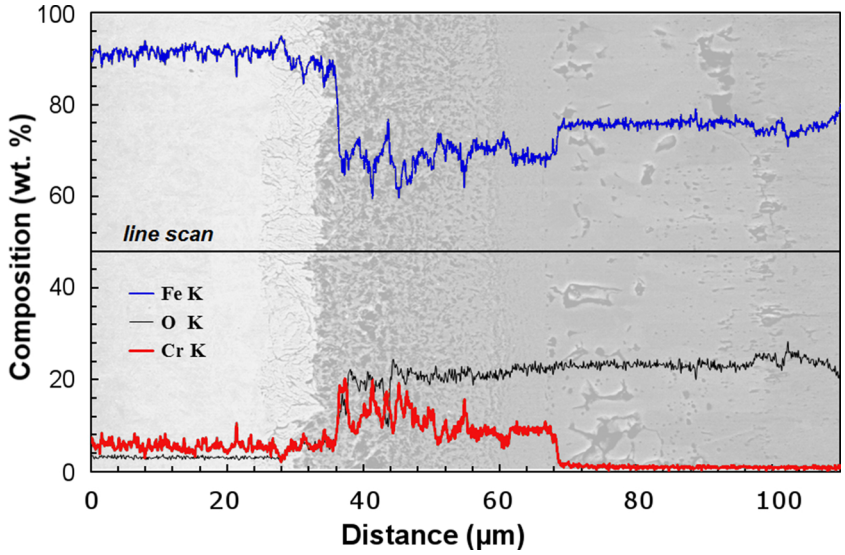

Fig. 3. Element concentration profiles (Fe, Cr and O) determined by EDS analyses through the oxide layer on the thermal aging sample at 650 °C during 100 h (the reader is referred to the online article for color version).

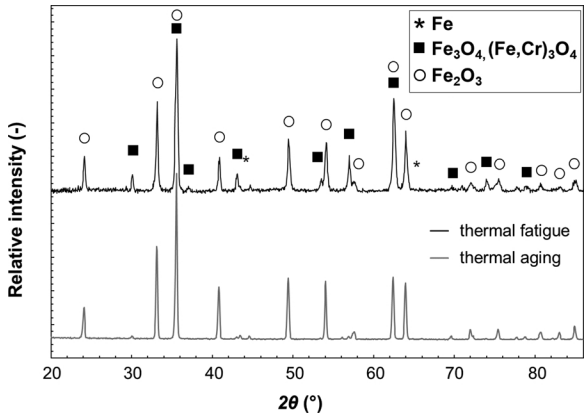

Fig. 4. XRD patterns of both thermally aged sample at 650 °C during 25 h and thermal fatigue specimen tested in air at T_{max} = 650 °C, ht = 1.5 s after 30,000 cycles (conventional 2θ acquisition mode with angular step size = 0.033°, integration time = 15 s, voltage = 40 kV, current = 40 mA).

stress). As for the pre-exponential coefficient k_0, it is close to 1.6 × 10^6 µm $s^{-1/2}$.

4.2.2. Cyclic conditions

In a first attempt, the oxide thickness δ_{ox} was reported as a function of the square root of the oxidation time t (estimated using Eq. 3), for thermal fatigue tests performed with various maximal temperatures T_{max} (Fig. 9a) and heating times ht (Fig. 9b). As no spallation was observed, the oxide thickness increases with increasing t and T_{max}. Since δ_{ox} is equal to zero at the beginning of the test, data can be adjusted by the least square method for each thermal fatigue condition, using Eqs. 1 and 2 where T is replaced by T_{max}. One could observe that the slope of the regression line differs from one test condition to the other, indicating that the apparent oxidation rate constant k_p is strongly T_{max}-dependent. Logically, for a same duration t, the total oxide layer was found much thicker when T_{max} was higher (especially above 600 °C). For example, after 100 h of thermal cycling, the maximum oxide thickness was about 9 µm when T_{max} = 650 °C, twice thinner at 600 °C and five times thinner at 500 °C. Compared to static isothermal tests, one could note that the apparent k_p is smaller under thermal fatigue (Tables 3 and 4). This was also concluded by Christl et al. [53] when comparing thermal aging and thermal cycling experiments performed

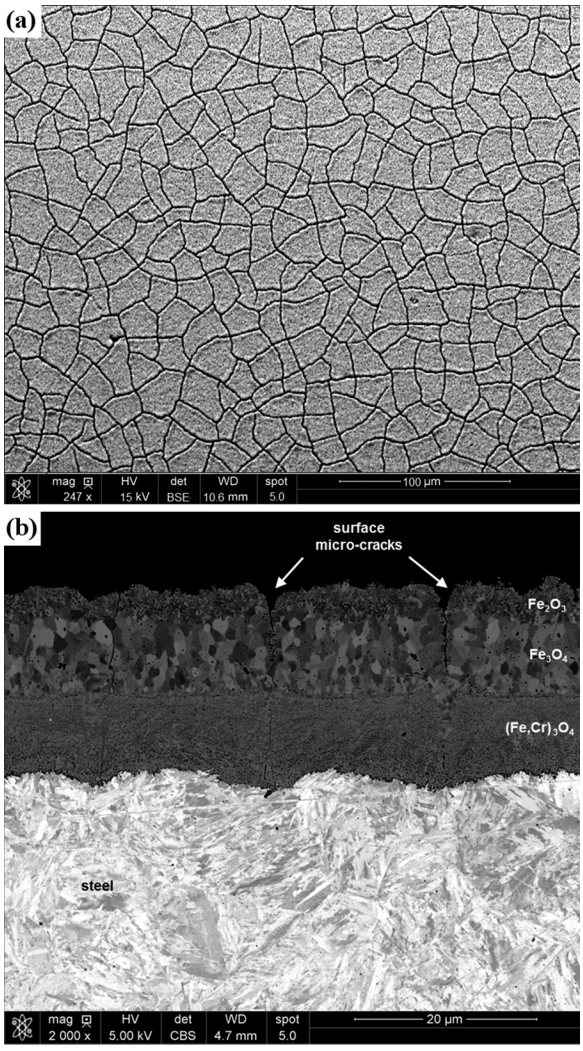

Fig. 5. SEM micrographs (backscattering mode) of a thermal fatigue specimen (T_{max} = 650 °C, ht = 1.5 s) after 30,000 cycles: (a) heat-checking network initiated in surface, (b) multi-layered oxide with a through-scale micro-crack observed in cross-section.

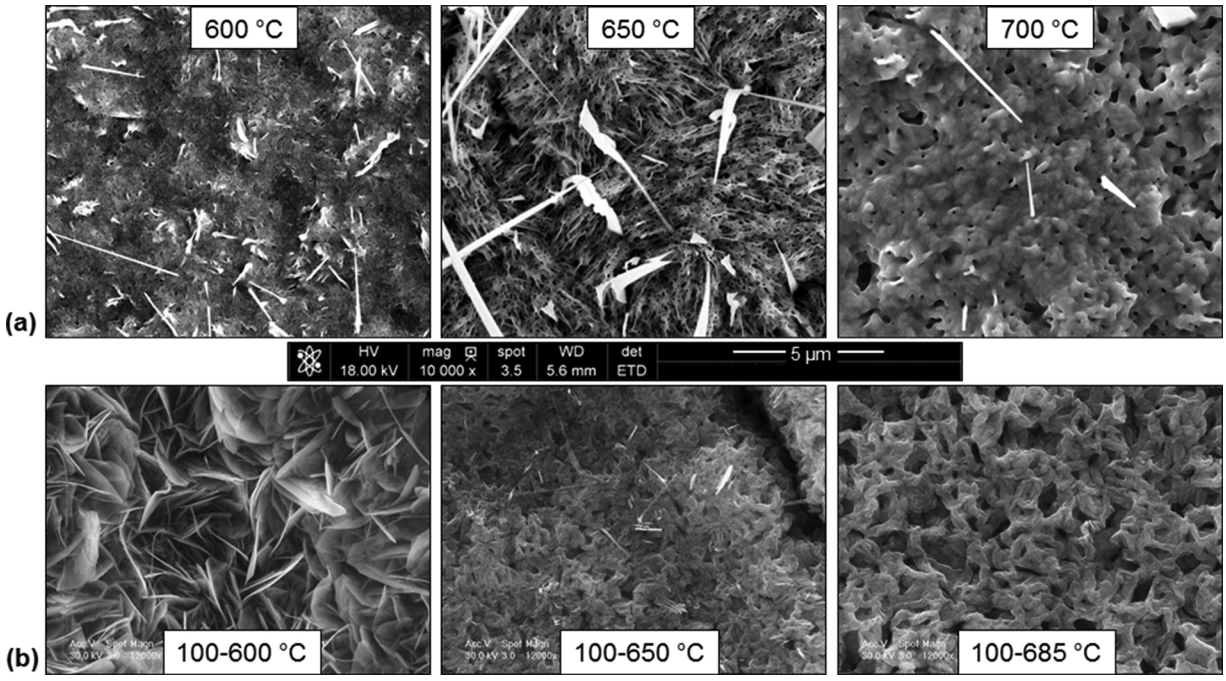

Fig. 6. SEM observations of the superficial hematite layer on 100 h thermal aging samples (a) and thermal fatigue specimens (b), for various temperatures / thermal cycles, showing different morphologies (the scale, provided by the 5 µm bar in the middle, is similar for all micrographs; the SEM observations were performed with an acceleration voltage comprised between 18 and 30 kV and a spot size of 3–3.5 µm).

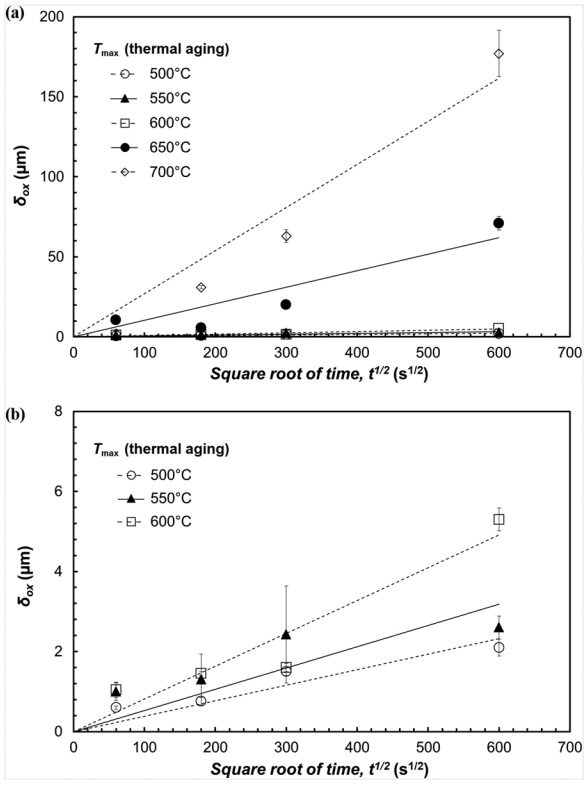

Fig. 7. (a) Parabolic oxidation kinetics (oxide thickness δ_{ox} vs. time t) determined from thermal aging tests between 500 and 700 °C, (b) enlarged y-axis to better show the oxidation kinetics from 500 to 600 °C.

Table 3
Apparent rate constants k_p determined from thermal aging tests performed at various temperatures (the coefficient of determination R^2 of the fit is indicated for each temperature).

Aging temperature (°C)	k_p (µm $s^{-1/2}$)	R^2
500	4.2×10^{-3}	0.89
550	7.2×10^{-3}	0.78
600	9.6×10^{-3}	0.95
650	9.1×10^{-2}	0.89
700	2.4×10^{-1}	0.95

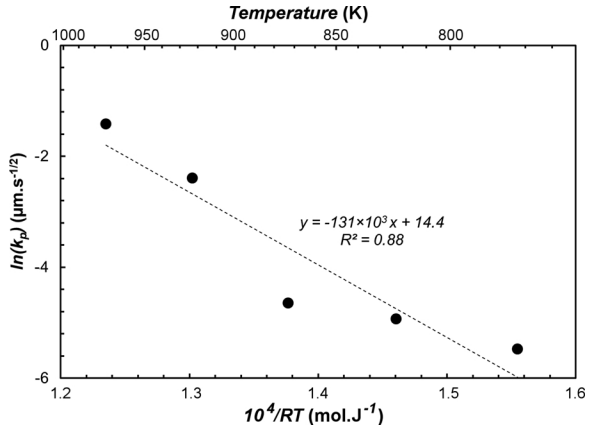

Fig. 8. Determination of the activation energy Q in isothermal conditions, from Arrhenius law.

on 2.25Cr-1Mo steel in air. In the same way, Daffos [49] reported that the oxide layer obtained on a X38CrMoV5 specimen tested under low cycle fatigue (LCF) at 650 °C was about ten times thicker than under thermal fatigue (for the same T_{max} and similar test durations). In addition, Fig. 9b indicates that, for the thermal fatigue tests performed with a same T_{max} (650 °C) but different heating periods (ht), the oxidation kinetics also depends strongly on the cycle time (t_{cy}). Still considering 100 h of testing, the oxide layer was almost two times thicker when the heating rate was reduced by a factor four (i.e. when ht changes from 1.5 to 6.3 s). Table 4 clearly reported that k_p is a function

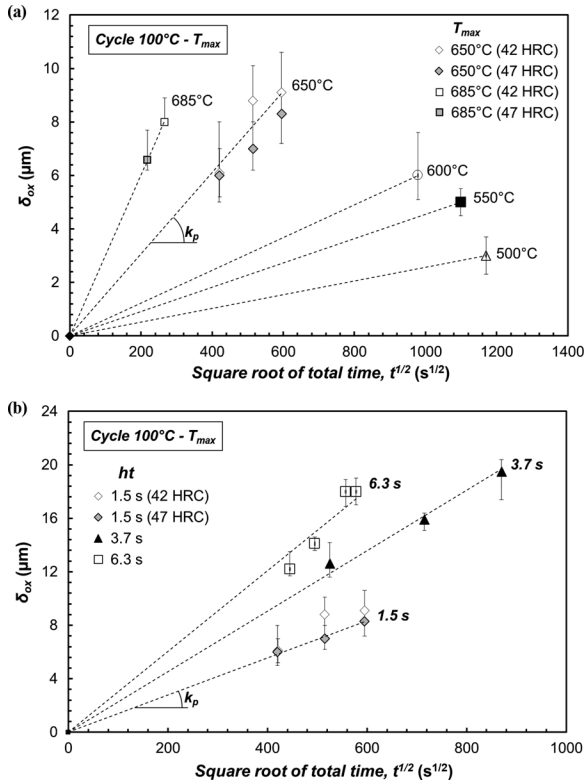

Fig. 9. Cyclic oxidation kinetics: variation of the oxide thickness versus the square root of time, for various (a) T_{max}, and (b) *ht* (when T_{max} = 650 °C).

Table 4
Apparent oxidation rate constants k_p determined by considering the total time of the test, for various thermal fatigue test conditions (the coefficient of determination R^2 of the fit is indicated for each condition).

T_{max} (°C)	*ht* (s)	t_{cy} (s)	k_p (µm $s^{-1/2}$)	R^2
500	0.7	13.7	2.6×10^{-3}	N/A
550	0.9	15.4	4.5×10^{-3}	N/A
600	1.3	16.0	6.3×10^{-3}	N/A
650	1.5	18.2	1.4×10^{-2}	0.77
650	3.7	25.7	2.2×10^{-2}	0.97
650	6.3	36.5	3.0×10^{-2}	0.84
685	1.8	23.6	3.0×10^{-2}	N/A

Note: N/A means non-applicable.

of T_{max} and t_{cy}, and may vary by a factor twelve when T_{max} changes from 500 to 685 °C.

The strong dependence of k_p on thermal fatigue parameters (i.e. T_{max} and t_{cy}) defeats the straightforward simplification of transposing T_{max} instead of T and the total cycle time for t. In fact, Eq. 1 should be expressed to account for the time spent at high temperature rather than including the time spent at low temperature, to have a chance to fit the data whatever the thermal fatigue condition. The dependence with t_{cy} for a fixed T_{max} (here 650 °C) could be explained by the total time spent at high temperature, which was much larger in thermal aging compared to thermal fatigue experiments. Similarly, the total time spent at high temperature also increased when t_{cy} increased in the present investigation. To better compare data obtained under various thermal cycles, an "equivalent oxidation time" needs to be used. This was the purpose of the AnT²COK model proposed in Section 2 and whose application is shown in the following section.

4.3. Application of the AnT²COK model

In a first approach, the AnT²COK model was employed in order to take into account the "equivalent oxidation time" during the thermal transient cyclic conditions, using the activation energy (Q = 131 kJ.mol^{-1}) and frequency factor (k_0 = 1.6×10^6 µm.s$^{-1/2}$) determined under isothermal conditions. The term A in Eq. 13 actually represents the "equivalent oxidation time" for a cycle, while the factor A/t_{cy} expresses the ratio between the equivalent oxidation time and the cycle time. The model was expected to normalize all the thermal fatigue test conditions, regardless whether the maximum temperature T_{max} or the heating rate *ht* was changed. Should the assumptions set in Section 2 be verified, all the curves representing the oxide thickness should then align on one parabolic law.

In Fig. 10, the oxide thickness δ_{ox} (normalized by $\sqrt{A/t_{cy}}$) was plotted versus the square root of time according to Eq. 11, for all thermal fatigue test conditions. One can see that all data retrieved from the thermal fatigue tests performed at T_{max} > 550 °C gather in a single linear curve, regardless of T_{max} or *ht*. This confirms that the AnT²COK model proposed is a step improvement for the oxidation kinetics in cyclic conditions under fully transient thermal conditions. The slope of the linear curve should correspond to the pre-exponential factor k_0, as experienced in the thermal fatigue conditions. The estimated coefficient is close to 4.6×10^6 µm.s$^{-1/2}$, which is larger than that measured in thermal aging conditions (1.6×10^6 µm.s$^{-1/2}$) but of the same order of magnitude. We believe that k_0 derived from Fig. 10 is not just an apparent k_0 as the ones estimated in the simpler models, but that it represents the true frequency factor which can be related to diffusion paths or other physical features due to thermo-mechanical stresses. In that sense, our interpretation is that the thermal fatigue specimens exhibit denser diffusion paths than isothermal unloaded specimens, due to the recurrent expansion/contraction of the oxide and substrate.

However, two points corresponding to tests performed at T_{max} = 500 and 550 °C deviate strongly from the regression line, suggesting that the AnT²COK model would not be applicable for lower temperatures. In our attempt to understand which of the assumptions were no longer verified, we retained the following three hypotheses:

1 The pre-exponential factor k_0 may not be the same at low and high temperatures. Since k_0 relates to the diffusion path density, it is linked to the morphology of the oxide layers, and it was previously shown that the morphology of the outer hematite layer tended to change beyond T_{max} = 600 °C (Fig. 6). Therefore, it would not be surprising to observe two domains of oxidation behavior below and above 600 °C. Interestingly, such a statement could also be noticed when looking at the evolution of the parabolic constant as a function of the temperature (Fig. 8). The linear fit used to take into account the temperature dependence of k_p underestimated the experimental parabolic constant for temperatures below 550 °C.
2 It could be argued that the activation energy Q may also change at different temperatures. Considering an averaged activation energy could only lead to a better fit at high temperature, which dominates the" effective oxidation time" even if the activation energy may be slightly lower (due to $1/RT$ in the exponential).
3 Both k_0 and Q could change at the same time.

These three hypotheses will be discussed in Section 5.

The application of the AnT²COK model clearly demonstrated the parabolic dependence of the normalized oxide thickness δ_{ox} as a function of the time. However, the value of the pre-exponential factor k_0^{cycl} (determined from thermal transient cyclic oxidation tests) was slightly higher than k_0^{isoth} (found in isothermal conditions). Therefore, the validity of the analytical simplification of the model was compared to an incremental simulation calculating the variation of oxide thickness at each acquisition time and for all the cycles, based on Eq. 5 and the COSP-type model (without weight loss). In Fig. 11, the oxide thickness determined with the AnT²COK model (Eq. 11) was plotted as a function of the thickness calculated from the incremental model. The two models are in very good agreement (regression coefficient and slope both close

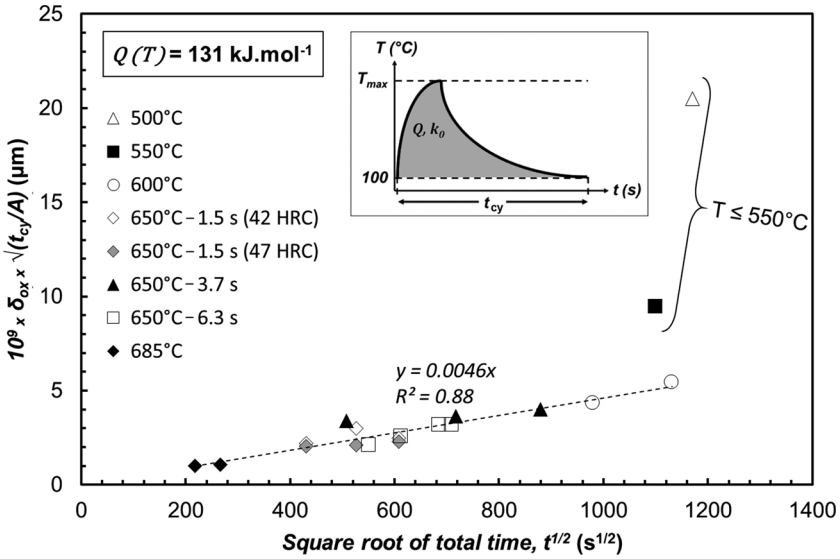

Fig. 10. Application of the AnT²COK model of cyclic oxidation kinetics for various thermal fatigue conditions, considering an activation energy of 131 kJ.mol^{-1}.

to 1). Thus, the AnT²COK model is particularly well suited for thermal transient calculation and offers an important time calculation gain compared to the incremental model ($t^{calc}_{AnT2COK} = t^{calc}_{incremental}/N$), especially for long term experiments.

5. Discussion

5.1. Equivalent oxidation time

The "equivalent oxidation time", as defined by the AnT²COK model, is given by the term *A*. As shown in Table 5, this equivalent time is of the order of 10^{-19} to 10^{-15}s, which is very small compared to the cycle durations (13–36 s). Should this term be compared to the oxidation time in isothermal conditions (with *N* cycles of 1 s for example), *A* would actually be mathematically equal to:

$$A = t_{cy}.\ exp\left(-\frac{2Q}{RT}\right),\ with\ t_{cy} = 1s \tag{14}$$

and the oxide growth law would be given by Eq. 11.

Therefore, from a numerical point of view, *A* should be of the order of magnitude of *exp* (*-2Q/RT*), hence the smallness of the "equivalent oxidation time" used in the AnT²COK model. From discussions and literature, it could be argued that another "equivalent oxidation time" could have been used. For example, the time spent at high temperatures instead of the full cycle time as formalized by the AnT²COK model could be very valuable. The notion of "time spent at high temperatures" was inspired from the COSP-type models and related experiments, where thermal cycles with a long dwell time are applied and the contribution

Table 5
Calculated values of *A* in Eq. (11), for various thermal fatigue test conditions.

T_{min} (°C)	T_{max} (°C)	*ht* (s)	Φ_{max} (MW/m²)	t_{cy} (s)	*Q* (kJ. mol^{-1})	*A* (s)
100	500	0.7	4.75	13.7	131	4.0×10^{-19}
100	550	0.9	4.75	15.4	131	6.4×10^{-18}
100	600	1.3	4.75	16.3	131	6.4×10^{-17}
100	650	1.5	4.75	18.5	131	3.3×10^{-16}
100	650	3.7	2.78	25.7	131	5.6×10^{-16}
100	650	6.3	2.13	36.3	131	1.3×10^{-15}
100	685	1.8	4.75	23.8	131	1.4×10^{-15}

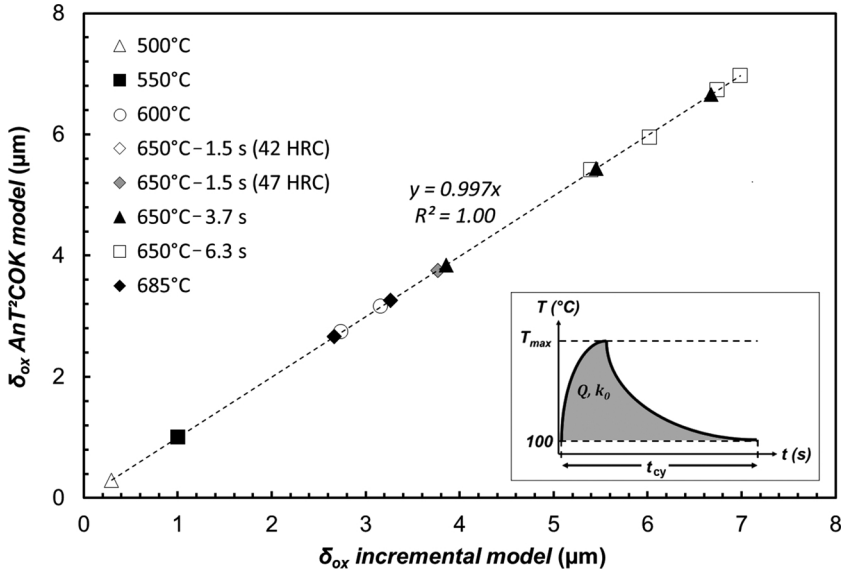

Fig. 11. Comparison of the AnT²COK model (Eq. 11) with an incremental simulation (Eq. 5), showing a strong correlation between the two calculation techniques.

of low temperature exposures is thus negligible (the transient term is ignored in [46]). In our fully transient tests, the definition of "time spent at high temperature" was not as straightforward. As mentioned in Section 2, it had commonly been accepted in our laboratory that oxidation below 300 °C was negligible.

By reporting the oxide thickness (δ_{ox}) as a function of the time spent above 300 °C (t'), the data collected from thermal fatigue tests performed at T_{max} = 650 °C with various t_{cy} - that were scattered in Fig. 9b - are now fitted by a single regression line (Fig. 12). In such conditions, the calculated apparent oxidation rate constant ($k_{p'}$, reported in Table 6) was in average three times higher than the previous k_p values determined using t instead of t' (Table 4). As previously done for thermal aging experiments, the apparent oxidation kinetics ln(k_p') could be plotted versus T_{max}, as shown in Fig. 13 which revealed a linear trend with a good coefficient of determination (R^2 = 0.94). Consequently, an apparent activation energy Q' of 62.4 kJ.mol^{-1} and a frequency factor k_0' of 132 µm.s$^{-1/2}$ could be estimated. With this definition of "equivalent oxidation time", the time itself was closer to the effective cycle time (with a ratio to t_{cy} close to 10^{-1} instead of 10^{-17} to 10^{-19}). But as a result, the ratio of the apparent frequency factor k_0' to that of isothermal tests was drastically reduced by a factor 10^4, whilst the apparent activation energy was reduced by about two.

In the end, the definition of the "equivalent oxidation time" in the AnT^{2}COK model has the merit of taking into account the physical mechanisms of oxide growth and allows to conserve the same activation energy and similar kinetic diffusion coefficients, even if the equivalent time is very different to the real accumulated time in the tests.

5.2. *Effect of a change of the frequency factor k_0*

Another key assumption of the AnT^{2}COK model was that the frequency factor k_0 was constant within the temperature range in cycling conditions. Should this not be the case, the model would not make much sense. k_0 representing the diffusion path density, it should therefore reflect the type of microstructure formed during the cycling. It is not meant to change within each cycle due to a change in temperature.

There is, however, no reason to believe that k_0 should be exactly the same as in isothermal conditions. Fig. 6a indeed revealed that the microstructure of the superficial oxide was changing with the isothermal test temperature. During a thermal fatigue test, which screens the whole temperature range covered in isothermal tests, there was expectancy that the microstructure - and therefore k_0 - would be different.

Table 6
Apparent oxidation rate constants k_p' determined by considering the time spent at high temperature (i.e. above 300 °C), for various thermal fatigue test conditions (the coefficient of determination R^2 of the fit is indicated for each condition).

T_{max} (°C)	ht (s)	time above 300 °C (s)	k_p' (µm s$^{-1/2}$)	R^2
500	0.7	1.7	9.5 10^{-3}	N/A
550	0.9	2.4	1.4 10^{-2}	N/A
600	1.3	4.3	1.67 10^{-2}	N/A
650	[1.5 – 6.3]	5.3-13.8	4.30 10^{-2}	0.98
685	1.8	7.1	6.75 10^{-2}	N/A

Note: N/A means non-applicable.

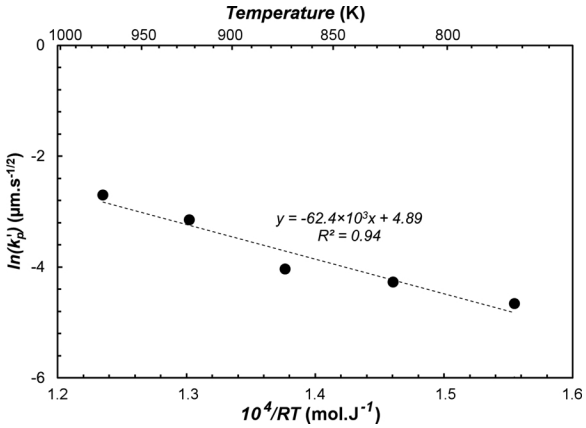

Fig. 13. Determination of an apparent activation energy Q' in the model based on the "dwell time", from an Arrhenius law.

As a matter of fact, Fig. 6b showed that the microstructure changed from low temperature tests to the higher ranges (especially between 600 and 650 °C), but it also showed that the microstructures can be very different between an isothermal test at T and a cyclic test at the same maximum temperature. This is the reason why k_0 was left as the only "free parameter" of the AnT^{2}COK model, when Q was fixed to the same value as for isothermal tests.

For all the tests performed above 550 °C, the good fit of the points after the normalization by the AnT^{2}COK model (Fig. 10) is a strong indicator that the diffusion path density is the same in all tests and slightly larger than in isothermal conditions. Assuming that the

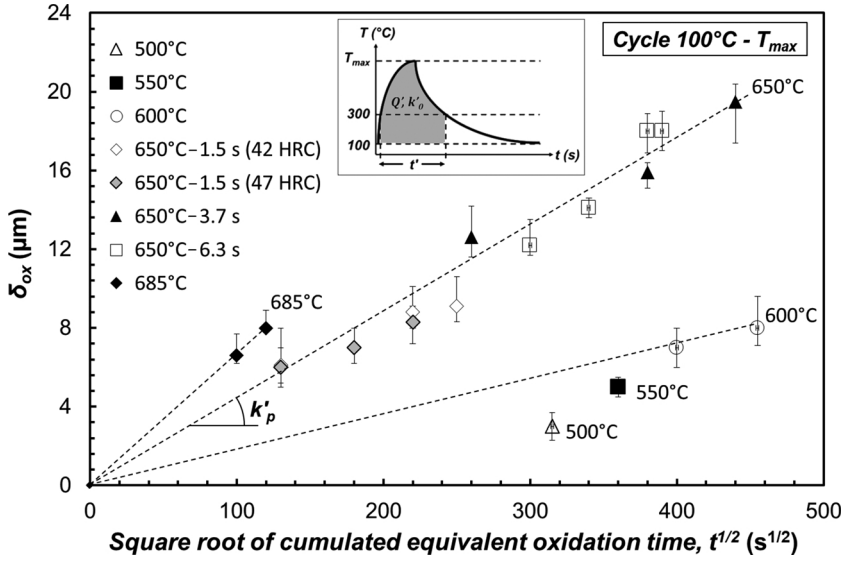

Fig. 12. Oxide thickness versus the square root of cumulated equivalent oxidation time spent between 100 °C and T_{max}, for various thermal fatigue test conditions.

activation energy is indeed not affected by the thermal cycling, it would mean that the cycling condition has contributed to increasing the diffusion path density.

With regard to the points at 500, 550 and 600 °C, all may be seen aligned with a very steep slope, suggesting a much higher diffusion path density than for higher temperatures. This could be understood, as the upper oxide layer tends to consist of many needles, leaving more paths for oxygen diffusion. However, the line does not intercept the origin of the graph, which is a strong deviation from the model (since the oxide thickness is supposed to be nil at the first cycle).

We can deduce that the assumption of a constant pre-exponential factor k_0 for tests above 550 °C stands, but that a change of k_0 alone cannot explain the misalignment of low temperature points. The answer must be found in a combination of a change of Q and k_0 at low temperatures.

5.3. *Effect of a change of activation energy Q*

One of the key assumptions of the AnT²COK model was that the activation energy of the oxide growth at each time step was the same as the isothermal activation energy, and it was assumed to be constant. One wonders what would happen if cyclic activation energy was different or not constant over the whole cycle.

By testing the sensitivity of the AnT²COK model to the value of activation energy, we found that a change of $+/-30\,\mathrm{kJ\,mol^{-1}}$ could have a detrimental effect. An activation energy lower than expected would have dispersed points at 600 °C beyond acceptable, while the other points were found aligning (even for 500 and 550 °C). With higher activation energy, alignment would still be acceptable for data above 550 °C, but not for lower temperatures. Even with a much larger value of Q ($200\,\mathrm{kJ\,mol^{-1}}$), the alignment was preserved but the slope (and therefore the estimated k_0) proved to increase dramatically (from 4×10^6 to 3×10^{10} $\mu m\,s^{-1/2}$). As a result, should the activation energy in thermal cycling be increased by more than $30\,\mathrm{kJ\,mol^{-1}}$, it should have been detected by a loss of fit. On the contrary, should Q be reduced by the thermal cycling, the AnT²COK model may not be able to detect the change (a higher value of Q than required would have been used). Moreover, it may have been possible for the effective activation energy to be slightly larger, and for the frequency factor k_0 to have been the same as the one found in isothermal conditions (but not without a slight loss of fit).

The reason why we chose to use the same activation energy than in isothermal conditions is linked to observations made by other researchers in our laboratory, after high temperature fatigue and thermo-mechanical fatigue tests on the same tool steels. Oudin [48] and Daffos [49] found that Q remained the same in thermal aging, isothermal fatigue conditions and thermo-mechanical fatigue, and further that the stress levels in low cycle fatigue did not affect its value. This was a confirmation of Engler-Pinto's previous findings for the thermo-mechanical fatigue of superalloys, that the oxidation kinetics was driven by the applied strain, but remained unchanged below a critical strain value [54]. Given that thermal fatigue tests are closer to the conditions applied in high cycle fatigue, it was fair to assume that the activation energy should not be affected more than in low cycle fatigue (performed with larger stresses and strains than in high cycle fatigue).

It may be argued that the activation energy is not constant in the temperature range covered by the thermal cycles. This argument derives from Figs. 8 and 10, which seem to highlight two domains for temperatures below or above 550–600 °C. Should this observation still be true in thermal cycling conditions, it would have been possible for the AnT²COK model to be adapted with integration in parts: with low activation energy (Q_l) for low temperatures, and higher value (Q_h) for higher temperatures. Mathematically, it would still be valid.

The model was re-applied with the integral, Eq. (13), being the sum of three integrals:

- from the beginning of the cycle to the point it reaches the transition temperature, with Q_l for activation energy;
- from the transition temperature to the maximum and back to the transition temperature on the way down, with Q_h for activation energy; and
- from the transition temperature to the end of the cycle, with Q_l for activation energy.

Attempts were made to try to fit all points (even those below 550 °C) by running calculations in which numerous sets of transition temperature, Q_l and Q_h, were tested. The best fit ($R^2 = 0.88$) was found for a transition temperature of 550 °C, and for $Q_l = 123\,\mathrm{kJ.mol^{-1}}$ and $Q_h = 131\,\mathrm{kJ\,mol^{-1}}$, as illustrated in Fig. 14. Interestingly, 550 °C was also attributed to an abrupt change in coefficient of thermal expansion of some ferrous oxides, i.e. Fe_3O_4 and $(Fe,Cr)_3O_4$ (with $\alpha_{550°C} = 2 \times \alpha_{500°C}$), as reported by Schültze [51]. As can be seen in Fig. 14 wherein all thermal fatigue tests are represented, the data points fit on a single straight line with a coefficient of determination as good as in Fig. 10 (in which the points at 500 and 550 °C were not considered in the interpolation). It can also be noted that the slope of the fitting line is still of the same order of magnitude, with 4.0×10^6 $\mu m\,s^{-1/2}$. This is consistent with data obtained in isothermal conditions. We are not

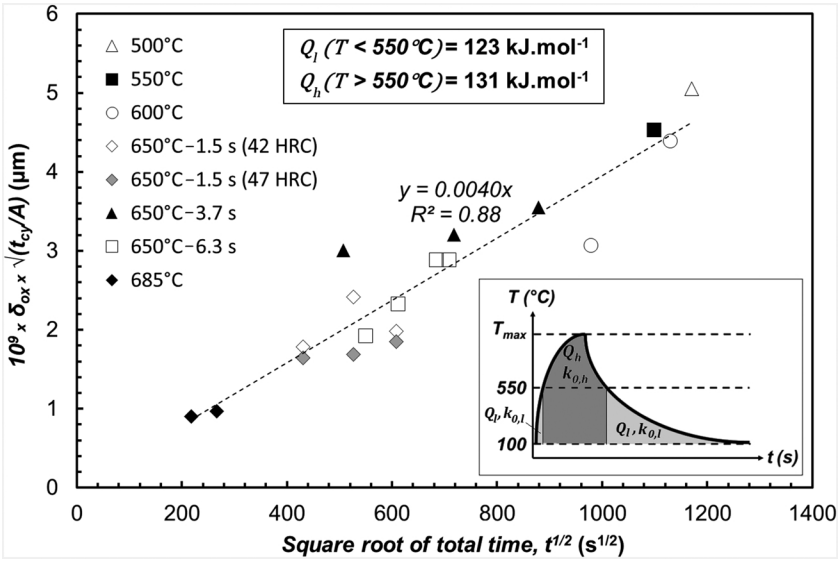

Fig. 14. Application of the AnT²COK model for various thermal fatigue conditions, considering two different values of activation energy below ($Q_l = 123\,\mathrm{kJ.mol^{-1}}$) and above 550 °C ($Q_h = 131\,\mathrm{kJ.mol^{-1}}$).

implying here that the values found to give the best fit are genuine, but rather that it is possible to apply the AnT²COK model with several steps of activation energy. Further studies would be required to confirm whether the anomaly observed at lower temperatures is actually due to a change in Q.

5.4. Effect of a change of both k_0 and Q

As pointed out in the previous section, Q may indeed change below 500–600 °C (as could be argued from Fig. 8). It is worth noting that the change of Q also means that k_0 changes as well, as the intersection of the fitting curve with the y-axis changes. In fact, one change rarely goes without the other.

As a general rule, a change of both oxidation kinetics parameters should have the following implications:

- a step change of Q could be managed as it was described in the previous section;
- a step change of k_0, whether at the same temperature as the step change of Q or not, would lead to a change of the fitting line. The line would still need to interpolate to the origin of the axis system (i.e. 0 µm for 0 s or 0 cycle).

In a general case, one would therefore expect to see the normalized data points aligning along two separate straight lines, intersecting the origin of the axes. Only in the most favorable cases, would one see all points aligning together, as in Fig. 14. This would correspond to the fortunate cases where the change in Q is not concomitant with a change in k_0.

5.5. On the statistical significance of the AnT²COK model

One may consider that the coefficient of determination obtained by applying the AnT²COK model to the thermal fatigue data was not very high ($R^2 = 0.88$), therefore questioning the validity of the model. A series of F-tests were used to estimate the validity of the linear fit in both Figs. 10 and 14.

The F-test was first performed for the series of points above 550 °C and for points on the linear trend line at the same x-coordinate. The results indicated a probability of more than 95% of the two distributions to have similar variance (based on 17 points and a cut-off value of 5%). The ratio of variance F was 1.07 versus a critical tail value of 2.33, thus validating the alignment of these points on the trend curve.

When the F-test was run including the low temperature points, the probability was less than 5% with a F ratio of 11.4 and a critical tail value of 2.22. Therefore, the fit for all points, including low temperatures, was found no longer valid.

Running the F-test on the model applied with two levels of activation energy (Fig. 14), it concluded on the validity of the curve fit (with a F ratio of 1.1 and a critical tail value of 2.21) when all the points were considered. Even a reduction to only low temperature points was still statistically valid (with $F = 7.2$ versus 19). As mentioned in Section 5.3, the purpose of curve fitting was to demonstrate that the AnT²COK model could be, mathematically speaking, extended to a situation with two levels of activation energy, rather than attempting to "reverse engineer" solution for the activation energy at low temperature.

As discussed in the previous section, the cause for the divergence of the low temperature points is certainly linked to a change of both the microstructure of the oxide layers (and therefore on k_0) and the activation energy Q at low temperature. At the current state of our research, however, it is not possible to conclude. Further oxidation tests at low temperatures, stressed and non-stressed conditions, combined with microstructural observations, would thus be required to confirm whether Q remains independent from the mechanical load at low temperatures (since experiments reported in [48] and [49] were all carried out above 550 °C).

6. Conclusion

A new model, called AnT²COK for Analytical Thermal Transient Cyclic Oxidation Kinetics, is proposed to account for oxide growth in cyclic conditions, based on the assumption that the growth rate obeys a parabolic law and that the activation energy is constant (at least by steps). This analytical model derives from the integration of the oxide growth at each time and temperature step. A series of experimental tests in isothermal and thermal fatigue conditions have been conducted to provide data, which are used to validate the model in the case of a X38CrMoV5 hot work tool steel.

The conclusions of the study are:

- The oxidation of hot work tool steels involves the growth of multiple layers, which grow in competition with each other.
- The kinetics of the isothermal oxidation, expressed as the overall oxide thickness, can be modeled with a parabolic law.
- The kinetics of the oxidation in fully transient cyclic conditions cannot be directly fitted with a single parabolic law. It was found that tests at different heating rates did not fit together.
- The AnT²COK model provides a very good fit for all tests conducted to temperatures higher than 550 °C, regardless of heating rates. The activation energy used for the fit was the one determined from the isothermal test conditions, i.e. 131 kJ.mol^{-1}
- A decomposition of the AnT²COK model's key integral into parts, accounting for high and low temperatures and the use of two activation energies in each part, was found to provide a good fit for all points, covering all test conditions. The transition temperature which gave the best result was 550 °C, and the best combination of activation energies was respectively 123 and 131 kJ.mol^{-1}. No other justifications of the value of 123 kJ.mol^{-1} is proposed at this point, other than a good fit. Interestingly, a transition in oxidation behavior was found at 550–600 °C.

Data availability

The raw/processed data required to reproduce these findings cannot be shared at this time due to technical or time limitations. It can be sent on request.

Acknowledgements

The authors would like to acknowledge the French Casting Technical Centre (CTIF) for supporting these activities and the Institut Clement Ader (ICA) for permitting on-going tests to finalise the article.

References

[1] G.A. Roberts, R. Kennedy, G. Krauss, Tool Steels, 5th ed., American Society for Metals, 1998.
[2] L.Å. Norström, N. Öhrberg, Development of hot-work tool steel for high-temperature applications, Metal. Technol. 8 (1) (1981) 22–26.
[3] J.P. Souchard, P. Jacquot, M. Buvron, Plasma overcarburizing of chromium steels for hot working and wear applications, Mater. Sci. Eng. A 140 (1991) 454–460.
[4] O. Barrau, C. Boher, R. Gras, F. Rézaï-Aria, Analysis of the friction and wear behavior of hot work tool steel for forging, Wear 255 (2003) 1444–1454.
[5] M. Pellizzari, M. Zadra, A. Molinari, Tribological properties of surface engineered hot work tool steel for aluminium extrusion dies, Surf. Eng. 23 (3) (2007) 165–168.
[6] K.D. Fuchs, Hot-work tool steels with improved properties for die-casting applications, Proceedings of the 6th International Tooling Conference Vol. 1 (2002) 15–22.
[7] C. Vergne, C. Boher, C. Levaillant, R. Gras, Analysis of the friction and wear behavior of hot work tool scale: application to the hot rolling process, Wear 250 (1) (2001) 322–333.
[8] G. Dour, Thermal stresses and distorsion in dies of die casting processes: a new normalised approach, Modell. Simul. Mater. Sci. Eng. 9 (2001) 399–413.
[9] F. Medjedoub, Détermination des Paramètres Influant sur le Phénomène d'Endommagement par Fatigue Thermique des Moules en Fonderie Sous Pression d'Aluminium, Ecole des Mines de Paris, 2004 PhD thesis.
[10] A. Hamasaiid, G. Dour, M.S. Dargusch, T. Loulou, C. Davidson, G. Savage, Heat-transfer coefficient and in-cavity pressure at the casting-die interface during high-pressure die casting of the magnesium alloy AZ91D, Met. Mater. Trans. A 39 (4)

(2008) 853–864.
[11] A. Hamasaiid, G. Wang, C. Davidson, G. Dour, M.S. Dargusch, Interfacial heat transfer during die casting of an Al-Si-Cu Alloy, Met. Mater. Trans. A 40 (13) (2009) 3056–3058.
[12] D.A. Spera, What is thermal fatigue? Thermal Fatigue of Materials and Components (1976).
[13] J. Sjöström, J. Bergström, Thermal fatigue in hot-working tools, Scand. J. Metal. 3 (2005) 221–231.
[14] R. Ebner, S. Marsoner, I. Siller, W. Ecker, Thermal fatigue behaviour of hot-work tool steels: heat check nucleation and growth, Int. J. Microstruct. Mater. Prop. 32 (2) (2008) 182–194.
[15] D. Klobčar, J. Tušek, B. Taljat, Thermal fatigue of materials for die-casting tooling, Mater. Sci. Eng. A 472 (1) (2008) 198–207.
[16] F. Medjedoub, G. Dour, S. Le Roux, P. Lamesle, M. Salem, P. Hairy, F. Rézaï-Aria, Experimental conditions and environment effects on thermal fatigue damage accumulation and life of die-casting steel X38CrMoV5 (AISI H11), Int. J. Microstruct. Mater. Prop. 3 (2–3) (2008) 336–349.
[17] M. Sundqvist, S. Hogmark, Effects of liquid aluminium on hot-work tool steel, Tribol. Int. 26 (2) (1993) 129–134.
[18] A. Molinari, M. Pellizzari, G. Straffelini, M. Pirovano, Corrosion behaviour of a surface-treated AISI H11 hot work tool steel in molten aluminium alloy, Surf. Coat. Technol. 126 (1) (2000) 31–38.
[19] P. Lamesle, M. Salem, S. Le Roux, G. Dour, F. Rézaï-Aria, Oxidation and corrosion effects on thermal fatigue behaviour of hot work tool steel X38CrMoV5 (AISI H11), Mater. Sci. Forum 595 (2008) 789–796.
[20] B. Miquel, S. Jean, S. Le Roux, P. Lamesle, F. Rézaï-Aria, Heat-checking of hot work tool steels, Eur. Struct. Integ. Soc. 29 (2002) 185–193.
[21] A. Persson, S. Hogmark, J. Bergstrom, Thermal fatigue cracking of surface engineered hot work tool steels, Surf. Coat. Technol. 191 (2005) 216–227.
[22] S. Le Roux, F. Medjedoub, G. Dour, F. Rézaï-Aria, Role of heat-flux density and mechanical loading on the microscopic heat-checking of high temperature tool steels under thermal fatigue experiments, Int. J. Fatigue 51 (2013) 15–25.
[23] C. Daffos, P. Lamesle, F. Rézaï-Aria, Fatigue-oxidation interaction models for life prediction of hot-forming tools steels under transient thermo-mechanical loadings, Int. J. Microstruct. Mater. Prop. 3 (2) (2008) 350–362.
[24] A. Oudin, P. Lamesle, L. Penazzi, S. Le Roux, F. Rézaï-Aria, Thermo-mechanical fatigue behaviour and life assessment of hot work tool steels, Eur. Struct. Integ. Soc. 29 (2002) 195–201.
[25] R.W. Neu, H. Sehitoglu, Thermomechanical fatigue, oxidation and creep: part I. Damage mechanisms, Metall Trans A 20A (1989) 1755–1767.
[26] R.W. Neu, H. Sehitoglu, Thermomechanical fatigue, oxidation, and creep: part II. Life prediction, Metal. Trans. A 20 (9) (1989) 1769–1783.
[27] J.R. Nicholls, M.J. Bennett, Cyclic oxidation – guidelines for test standardisation, aimed at the assessment of service behavior, Mater. High Temp. 17 (2000) 413–428.
[28] S. Baleix, G. Bernhart, P. Lours, Oxidation and oxide spallation of heat resistant cast steels for superplastic forming dies, Mater. Sci. Eng. A 327 (2002) 155–166.
[29] P. Bruckel, P. Lamesle, P. Lours, B. Pieraggi, In situ ESEM investigations of the oxide growth on hot-work tools steel: effect of the water vapour, Mater. High Temp. 20 (2003) 551–560.
[30] R.Y. Chen, W.Y.D. Yeun, Review of the high-temperature oxidation of iron and carbon steels in air or oxygen, Oxid. Met. 59 (5–6) (2003) 433–468.
[31] P. Bruckel, P. Lamesle, P. Lours, B. Pieraggi, Isothermal oxidation behaviour of a hot-work tool steel, Mater. Sci. Forum 461 (2004) 831–838.
[32] D. Laverde, T. Gomez-Acebo, F. Castro, Continuous and cyclic oxidation of T91 ferritic steel under steam, Corros. Sci. 46 (3) (2004) 613–631.
[33] Y.A. Min, X.C. Wu, W. Rong, L.I. Lin, L.P. Xu, Prediction and analysis on oxidation of H13 hot work steel, J. Iron Steel Res. Int. 13 (1) (2006) 44–49.
[34] A. Raffaitin, D. Monceau, E. Andrieu, F. Crabos, Cyclic oxidation of coated and uncoated single-crystal nickel-based superalloy MC2 analysed by continuous thermogravimetry analysis, Acta Mater. 54 (2006) 4473–4487.
[35] E. N'Dah, S. Tsipas, M.P. Hierro, F.J. Pérez, Study of the cyclic oxidation resistance of Al coated ferritic steels with 9 and 12% Cr, Corros. Sci. 49 (2007) 3850–3865.
[36] N.K. Othman, J. Zhang, D.J. Young, Temperature and water vapour effects on the cyclic oxidation behaviour of Fe–Cr alloys, Corros. Sci. 52 (9) (2010) 2827–2836.
[37] Y. Birol, Investigation of isothermal and cyclic oxidation of plasma-nitrided hot-work tool steel at elevated temperatures, Oxid. Met. 76 (5–6) (2011) 399–417.
[38] T. Liang, H. Guo, H. Peng, S. Gong, Cyclic oxidation behavior of an EB-PVD CoCrAlY coating influenced by substrate/coating interdiffusion, Chin. J. Aero. 25 (5) (2012) 796–803.
[39] J. Zhang, X. Peng, D.J. Young, F. Wang, Nano-crystalline coating to improve cyclic oxidation resistance of 304 stainless steel, Surf. Coat. Technol. 217 (2013) 162–171.
[40] D.J. Young, High Temperature Oxidation and Corrosion of Metals Vol. 1 Elsevier, 2008.
[41] J. Robertson, M.I. Manning, Limits to adherence of oxide scales, Mater. Sci. Technol. 6 (1) (1990) 81–92.
[42] M.M. Nagl, W.T. Evans, The mechanical failure of oxide scales under tensile or compressive load, J. Mater. Sci. 28 (23) (1993) 6247–6260.
[43] C.A. Barrett, A.F. Presler, COREST: A Fortran Computer Program to Analyze Paralinear Oxidation Behavior and Its Application to Chromic Oxide Forming Alloys, NASA Lewis Research Center, Cleveland, 1976 NASA-TN-D-8132 E-8432.
[44] C.E. Lowell, C.A. Barrett, R.W. Palmer, J.V. Auping, H.B. Probst, COSP: a computer model of cyclic oxidation, Oxid. Met. 36 (1–2) (1991) 81–112.
[45] J.L. Smialek, A deterministic interfacial cyclic oxidation spalling model, Acta Mater. 51 (2003) 469–483.
[46] D. Poquillon, D. Monceau, Application of a simple statistical spalling model for the analysis of high-temperature, cyclic-oxidation kinetics data, Oxid. Met. 59 (3-4) (2003) 409–431.
[47] J.H. Luo, Q. Zhang, F.B. Song, Computer simulation of the cyclic oxidation of the Al-Si coatings, Comput. Mater. Sci. 31 (2004) 220–224.
[48] A. Oudin, Thermo-mechanical Fatigue of Hot Work Tool Steels, PhD thesis Ecole des Mines de Paris, Albi, 2001.
[49] C. Daffos, Endommagement des Outillages de Forgeage Traités par Nitruration : Etude et Modélisation, PhD Thesis INSA de Toulouse, 2004.
[50] M. Salem, Étude de l'Endommagement par Fatigue Thermique des Moules de Fonderie Sous Pression d'Aluminium : Effet de l'Interaction avec l'Aluminisation et l'Oxydation, PhD Thesis Université Toulouse III-Paul Sabatier, 2009.
[51] M. Schütze, Protective Oxide Scales and Their Breakdown, John Wiley & Sons, 1999.
[52] G. Béranger, G. Henry, G. Sanz, Le livre de l'acier – Technique et documentation, Lavoisier, Paris, 1994.
[53] W. Christl, A. Rahmel, M. Schütze, Behavior of oxide scales on 2.25 Cr-1Mo steel during thermal cycling. I. Scales formed in oxygen and air, Oxid. Met. 31 (1–2) (1989) 1–34.
[54] C.C. Engler-Pinto Jr., Étude de l'Endommagement en Fatigue Thermomécanique De Superalliages à Base De Nickel, École Polytechnique Fédérale de Lausanne, 1996 PhD Thesis.